

## Supporting Information

### Dredging Sodium Polysulfides via Fe<sub>3</sub>C Electrocatalyst to Realize Improved Room-Temperature Na-S Batteries

Xiang Long Huang<sup>a\*</sup>, Tanveer Hussain<sup>e</sup>, Hanwen Liu<sup>d</sup>, Thanayut Kaewmaraya<sup>f</sup>,  
Maowen Xu,<sup>c\*</sup> Hua Kun Liu<sup>b</sup>, Shi Xue Dou,<sup>b\*</sup> Zhiming Wang<sup>a\*</sup>

<sup>a</sup> Institute of Fundamental and Frontier Sciences, University of Electronic Science and  
Technology of China, 610054, China

E-mail: [xlhuang\\_uestc@163.com](mailto:xlhuang_uestc@163.com); [zhmwang@uestc.edu.cn](mailto:zhmwang@uestc.edu.cn)

<sup>b</sup> Institute of Energy Materials Science, University of Shanghai for Science and  
Technology, Shanghai 200093, China

E-mail: [shi@usst.edu.cn](mailto:shi@usst.edu.cn)

<sup>c</sup> School of Materials and Energy, Southwest University, Chongqing 400715, China

E-mail: [xumaowen@swu.edu.cn](mailto:xumaowen@swu.edu.cn)

<sup>d</sup> Institute of Superconducting and Electronic Materials, University of Wollongong,  
New South Wales 2500, Australia

<sup>e</sup> School of Science and Technology, University of New England, Armidale, New South  
Wales 2351, Australia

<sup>f</sup> Department of Physics, Faculty of Science, Khon Kaen University, Khon Kaen 40002,  
Thailand

## **Experimental Details**

### **Materials synthesis**

#### **Synthesis of precursor**

600 mg of 2,5-dihydroxyterephthalic acid was fully dissolved into a glass container holding deionized water and dimethyl formamide (labelled as solution A). 1.008 g of zinc acetate dihydrate was fully dissolved into the other container holding deionized water and dimethyl formamide (labelled as solution B). Next, solution A was directly poured into solution B and continuously stirred for half an hour to form a yellow suspension. Then, the suspension was transferred into a Teflon-lined autoclave and hydro-thermally proceeded for 24 hours at 100°C. After naturally cooling down to the ambient temperature, the yellow precipitate was collected via high-speed freezing centrifugation, purified with ethanol for three times at least, and dried overnight at 80 °C in a blast drying oven. The yellow solid powder was MOF-74.

#### **Synthesis of HPC**

The MOF-74 was placed into a porcelain, transferred to a tubular furnace, and heated for 4.5 hours at 900°C under the protective Argon gas flow. The heating speed was 10 °C/min. After naturally cooling, the obtained black powder was HPC.

#### **Synthesis of Fe<sub>3</sub>C@HPC**

90 mg of HPC and 90 mg of FeCl<sub>3</sub> was poured into 10 ml of ethanol and stirred for 10 hours at least so that the HPC could fully adsorb iron ions. The mix solution was dried for 12 hours at 80°C in a drying oven. The as-produced Fe-contained HPC was further annealed for 3 hours at 900°C under the protective Argon gas flow. After cooling to room temperature, the Fe<sub>3</sub>C@HPC was obtained.

#### **Synthesis of HPC-S and Fe<sub>3</sub>C@HPC-S**

The S and Fe<sub>3</sub>C@HPC (or HPC) was mixed with a mass ratio of 1:1, fully grinded, and heated for 12 hours at 155°C in a closed container. After cooling, the Fe<sub>3</sub>C@HPC-S (HPC-S) was successfully fabricated.

#### **Polysulfide adsorption experiment**

A mixture of anhydrous sodium sulfide (Na<sub>2</sub>S) and sublimed sulfur with a molar ratio of 1:5 was added into a mixed organic solution of 1, 3-dioxolane (DOL) and diethylene glycol dimethyl ether (DIGLYME) (v:v = 1: 1) and violently stirred for 12 hours under the protection of Argon gas to generate a Na<sub>2</sub>S<sub>6</sub> solution with a concentration of 0.2 M. Then, the Na<sub>2</sub>S<sub>6</sub> solution was diluted to a suitable concentration to carry out adsorption experiment. 30 mg of HPC and Fe<sub>3</sub>C@HPC were added into the as-diluted Na<sub>2</sub>S<sub>6</sub> solution, separately. The Na<sub>2</sub>S<sub>6</sub> solution without any additives was used as a blank reference.

#### **Material characterization**

The morphologies and nanostructures of all the samples were observed via field emission scanning electron microscope (ZEISS, GeminiSEM 300) and transition electron microscope (Tecnai G2 F20 S-TWIN). The elemental distributions were collected by energy dispersive spectrometry (EDS). The crystal structures and chemical states of all the samples were analyzed employing an X-ray diffractometer (XRD) with Cu K-alpha radiation and X-ray photoelectron spectra (XPS, Thermo Scientific ESCALAB 250Xi), respectively. Raman spectra of all the samples were obtained via

InviaRefl (Renishaw, UK) with 532 nm laser light. The specific surface areas and pore distributions of all the samples were investigated by Brunauer-Emmett-Teller method (BSD PS2, China). The contents of compositions in the samples were estimated using thermogravimetric analysis (TG 209, Germany) at corresponding gas atmospheres.

### **Electrochemical characterization**

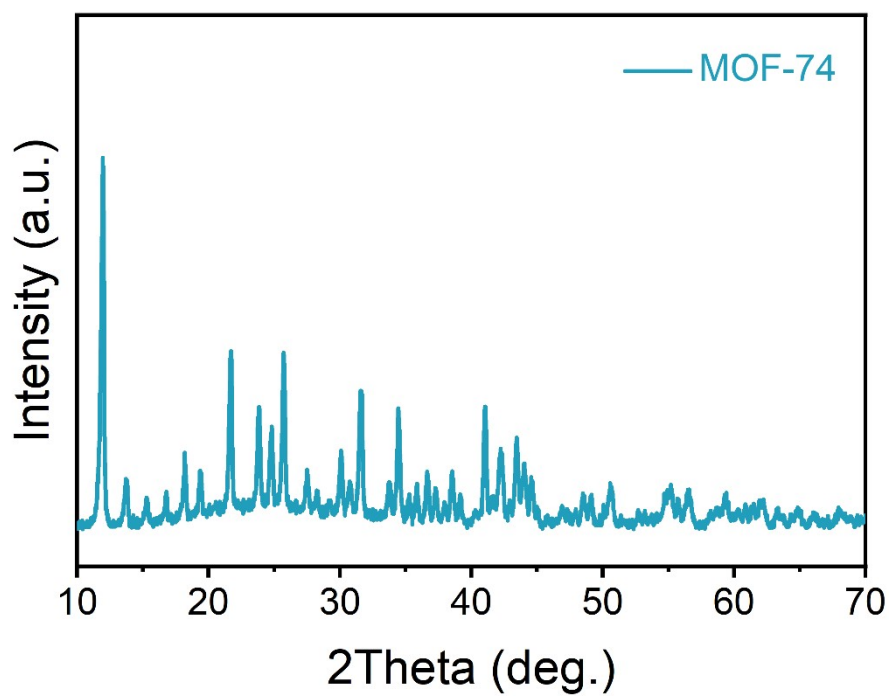
The prepared electrode materials, Ketjen black, and PVDF were mixed at a mass ratio of 8:1:1 in NMP solvent and grinded to a homogeneous slurry. The slurry was uniformly casted on a carbon-coated aluminum foil current collector, dried at 80°C for 12 hours in a vacuum oven to volatilize NMP. The diameter of disk electrodes was 12 mm. These disks made were assembled into 2032-type coin cells in an argon-filled glove box (oxygen/water content < 0.01 ppm). The diameter and thickness of the used sodium foils were 15.6 mm and 500  $\mu\text{m}$ , respectively. The glass fiber disc (Whatman, GF1820-125) with a diameter of 19 mm served as separators. The electrolyte was 1M  $\text{NaClO}_4$  dissolved into mixture solvent of EC and PC with 5% of FEC as an additive. The galvanostatic discharge-charge tests were conducted on a LAND instrument testing system under a room temperature. The voltage window employed was 0.8-2.8 V. CV curves were recorded on electrochemical workstation (Chenhua Instrument, CHI 660E) and EIS was also carried out on electrochemical workstation (Chenhua Instrument, CHI 660E) with a frequency range from 0.01 Hz to 100 kHz. The in-situ XRD analysis of coin cell was carried out on X-ray diffraction (XRD, Bruker, Advance D8A A25), with a Be foil sealing the cell, a current density of 0.1  $\text{A g}^{-1}$ , and a voltage window of 2.8-0.8 V.

### **Computational methods**

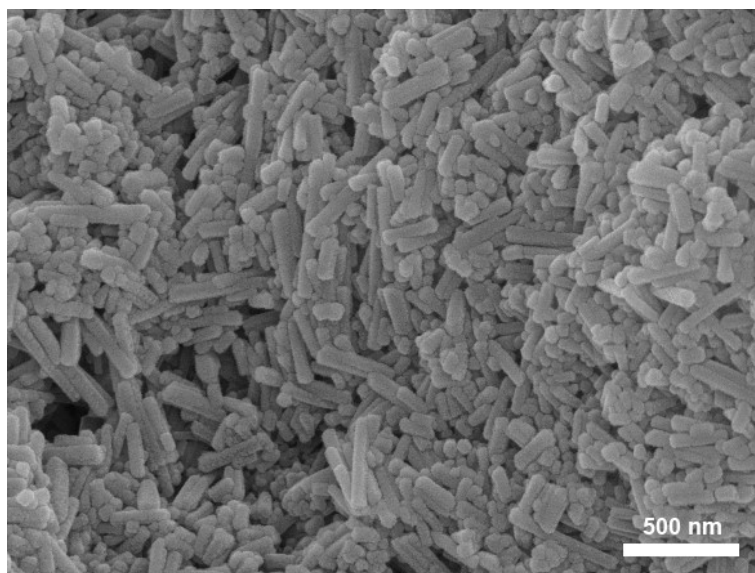
For studying the anchoring property of sodium polysulfides (NaPSs), spin-polarized density functional theory (DFT) calculations were employed as implemented in the Vienna *ab initio* Simulation Package (VASP) [1, 2]. Projector augmented wave (PAW) pseudopotential was used to study the electron-ion interaction, whereas Perdew-Burke-Ernzerhof (PBE) exchange-correlation functional within the generalized gradient approximation (GGA) was employed for the electron-electron interactions [3-5]. We used a cut-off energy value of 500 eV for the plane-wave basis set. Energy convergence criterion of  $10^{-6}$  was used throughout the calculations, whereas the structures were optimized until the force criteria of 0.001  $\text{eV}/\text{\AA}$  was met. Underestimation of GGA-PBE in evaluating the true binding energies were compensated by employing van der Waals (vdW) correction terms at DFT-D3 level [6]. Monkhorst-Pack scheme was adopted for the sampling of Brillouin zones with mesh sizes of 3 x 3 x 1, and 5 x 5 x 1 for structural optimization, and electronic properties, respectively [7]. Bader analysis was used to study the charge transfer mechanism [8]. To model  $\text{Fe}_3\text{C}$ -decorated nanorod-like porous carbon, we considered a 7 x 7 supercell of graphene ( $\text{C}_{98}$ ) and decorated it with  $\text{Fe}_3\text{C}$  ( $\text{Fe}_{12}\text{C}_4$ ) cluster. The  $\text{Fe}_3\text{C}@$ graphene was fully optimized before studying its interaction with NaPSs. Binding energies ( $E_b$ ) of the NaPSs ( $\text{Na}_2\text{S}$ ,  $\text{Na}_2\text{S}_2$ ,  $\text{Na}_2\text{S}_4$ ,  $\text{Na}_2\text{S}_6$ ,  $\text{Na}_2\text{S}_8$ ) with the  $\text{Fe}_3\text{C}@$ graphene were calculated by the following relation:

$$E_b = E (\text{Fe}_3\text{C}@ \text{graphene}-\text{Na}_2\text{S}_n) - E (\text{Fe}_3\text{C}@ \text{graphene}) - E (\text{Na}_2\text{S}_n)$$

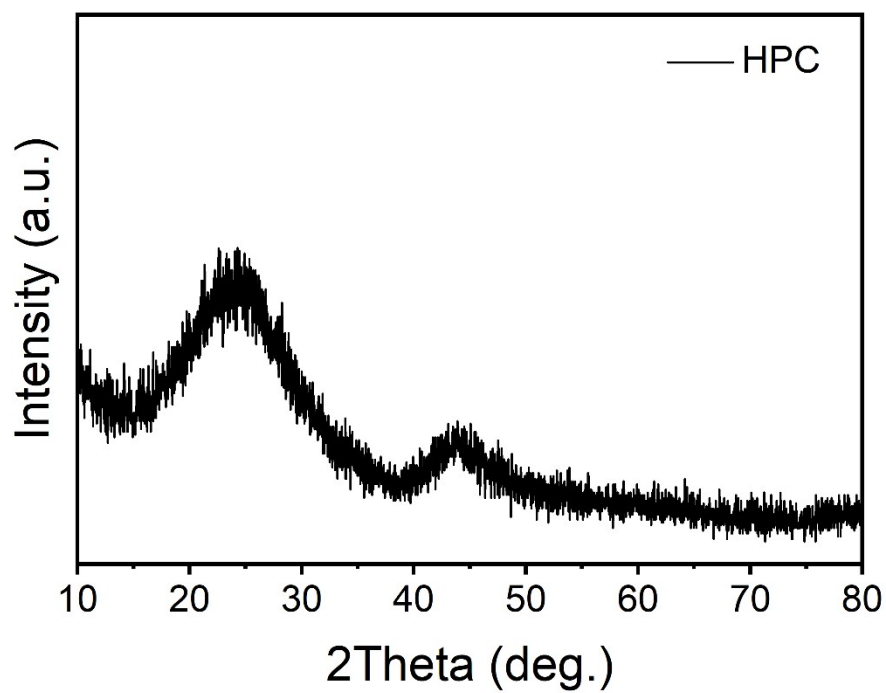
In above relation, first, second and third terms represent the total energies of  $\text{Na}_2\text{S}_n$  doped  $\text{Fe}_3\text{C}@$ graphene, bare  $\text{Fe}_3\text{C}@$ graphene and the total energies of the isolated  $\text{Na}_2\text{S}_n$  species, such as ( $\text{Na}_2\text{S}$ ,  $\text{Na}_2\text{S}_2$ ,  $\text{Na}_2\text{S}_4$ ,  $\text{Na}_2\text{S}_6$ ,  $\text{Na}_2\text{S}_8$ ), respectively.



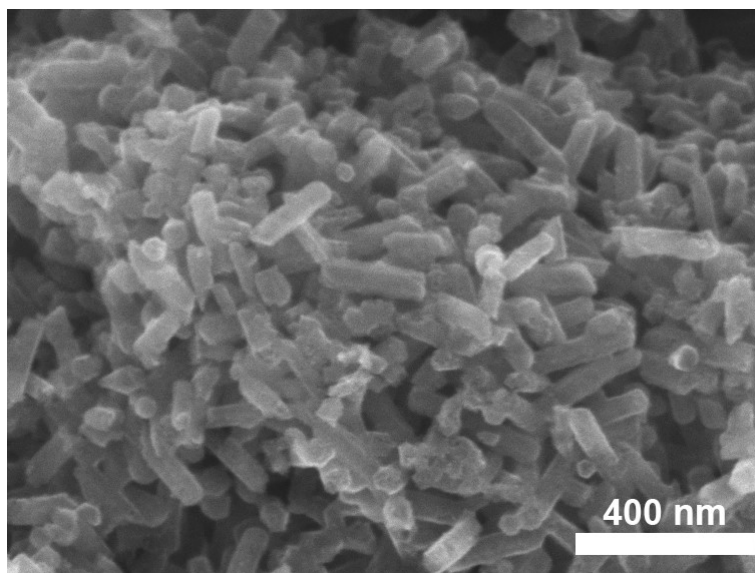
**Figure S1.** XRD pattern of MOF-74.



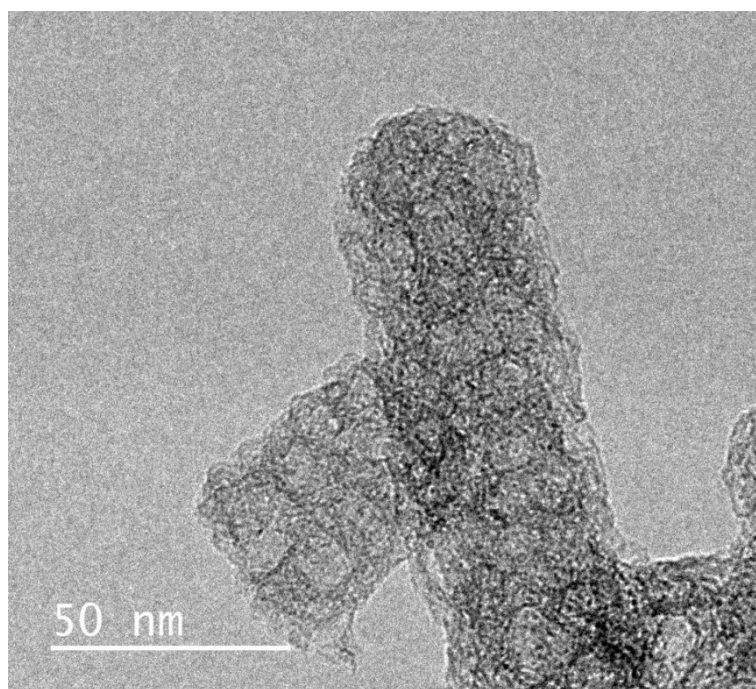
**Figure S2.** FESEM image of MOF-74.



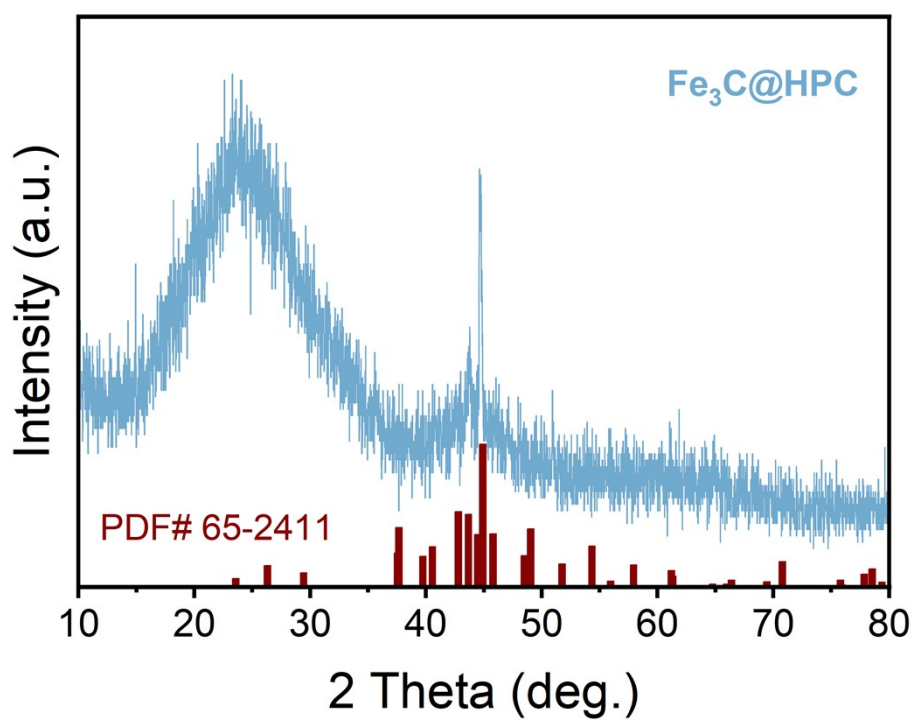
**Figure S3.** XRD pattern of the HPC.



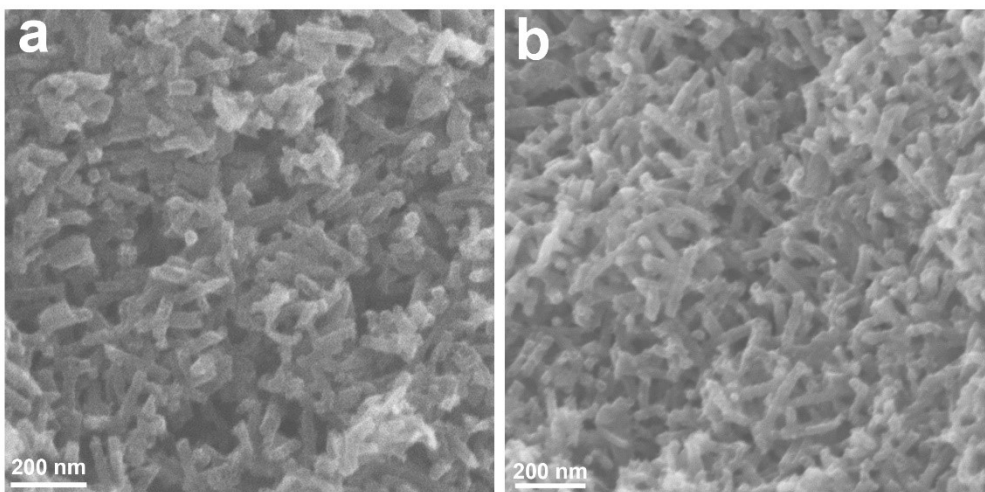
**Figure S4.** FESEM image of the HPC.



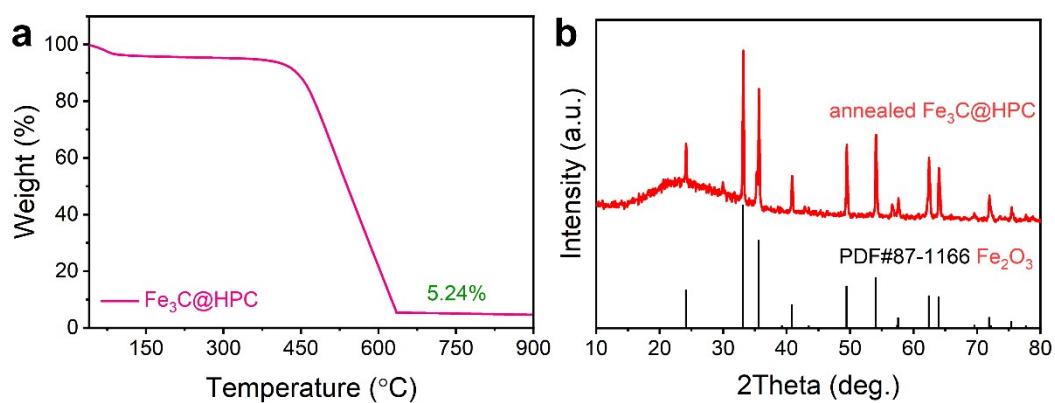
**Figure S5.** TEM image of the HPC.



**Figure S6.** XRD pattern of the Fe<sub>3</sub>C@HPC.

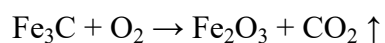
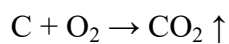


**Figure S7.** FESEM images of the  $\text{Fe}_3\text{C}@HPC$  (a) and  $\text{Fe}_3\text{C}@HPC-S$  (b).



**Figure S8.** TGA curve of the  $\text{Fe}_3\text{C}@HPC$  at air atmosphere and XRD pattern of the annealed the  $\text{Fe}_3\text{C}@HPC$ .

The  $\text{Fe}_3\text{C}@HPC$  reacts with air at high temperatures to generate carbon dioxide and ferric oxide. Carbon dioxide is taken away and ferric oxide is left. Based on Fe conservation, the content of  $\text{Fe}_3\text{C}$  in the  $\text{Fe}_3\text{C}@HPC$  can be calculated as 4%.



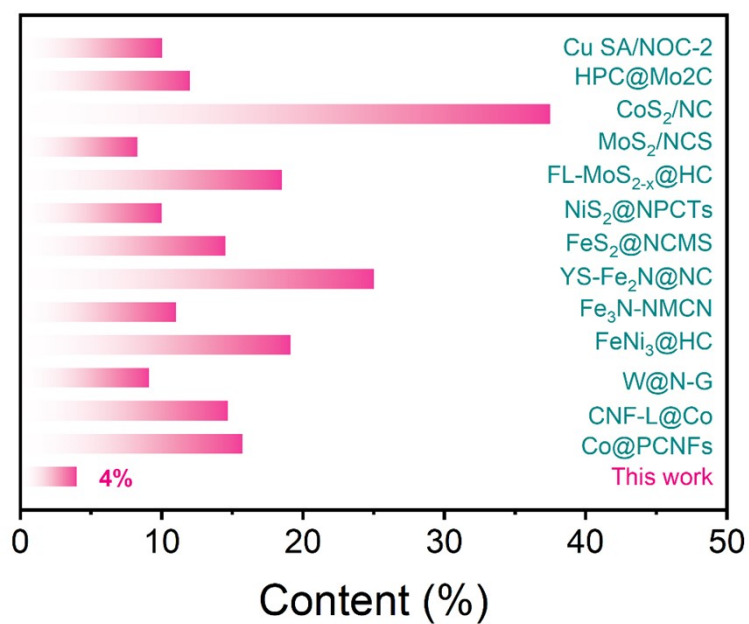


**Figure S9.** A comparison on electrocatalyst content into substrates for RT Na-S batteries.

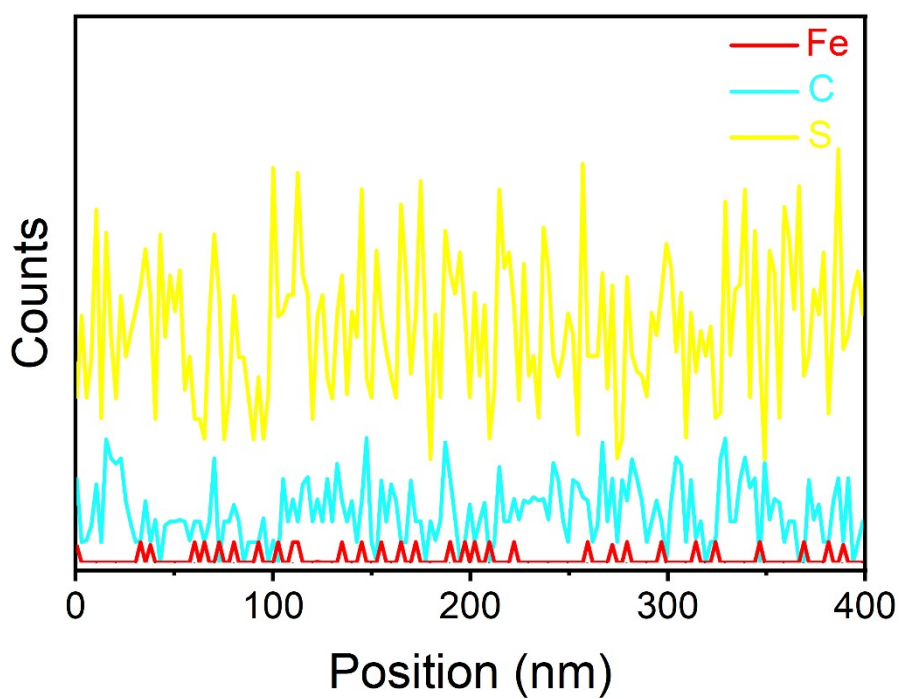


**Figure S10.** Linear elemental distributions of the Fe<sub>3</sub>C@HPC-S composite

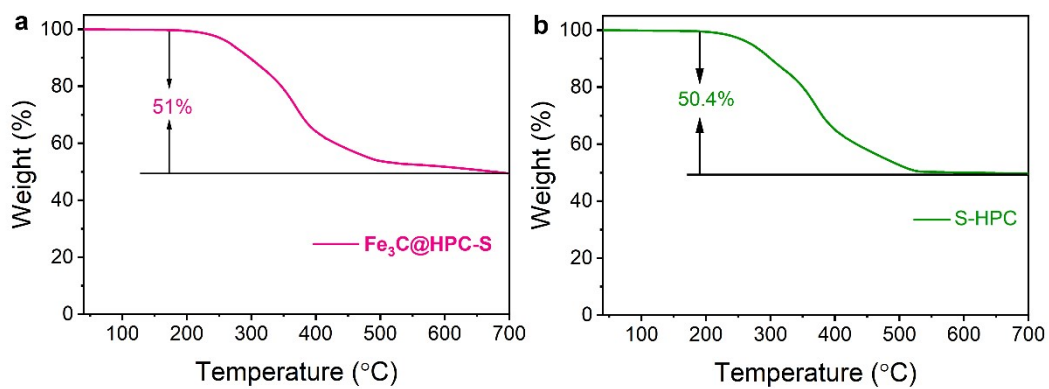


**Figure S11.** TGA curves of the  $\text{Fe}_3\text{C@HPC-S}$  and HPC-S composite.

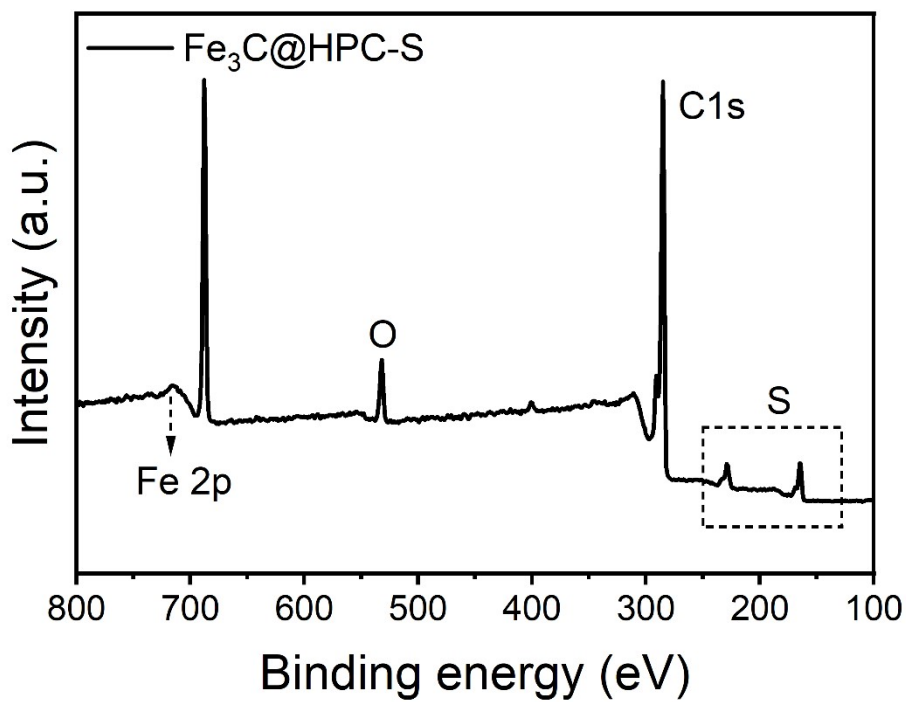


**Figure S12.** XPS spectra of the  $\text{Fe}_3\text{C@HPC-S}$ .

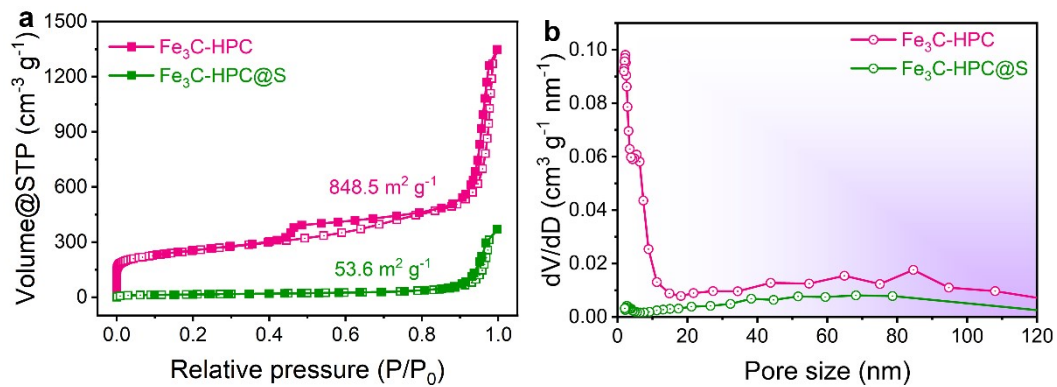


**Figure S13.** (a) Nitrogen adsorption/desorption isotherms and (b) pore-size distributions of the Fe<sub>3</sub>C@HPC and Fe<sub>3</sub>C@HPC-S composite.

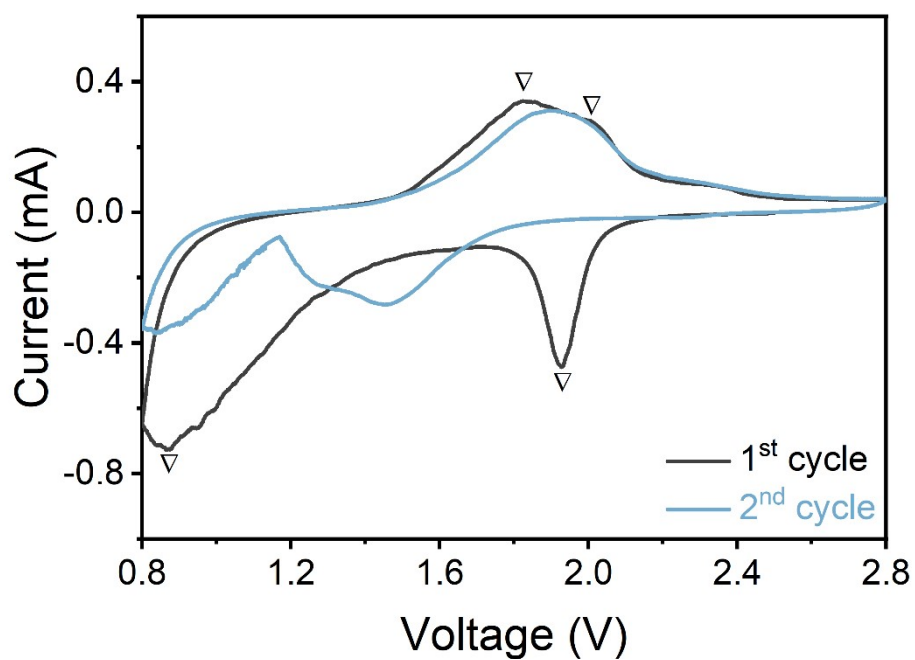


**Figure S14.** CV curves of the Fe<sub>3</sub>C@HPC-S at the first and second cycle.

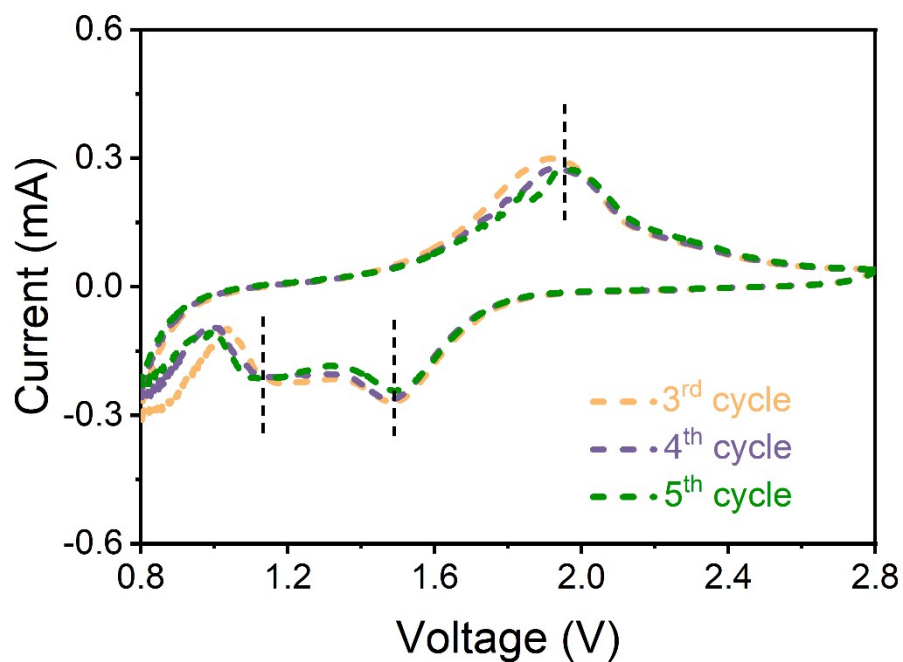


**Figure S15.** CV curves of the  $\text{Fe}_3\text{C}@\text{HPC-S}$  at the 3<sup>rd</sup>-5<sup>th</sup> cycle.

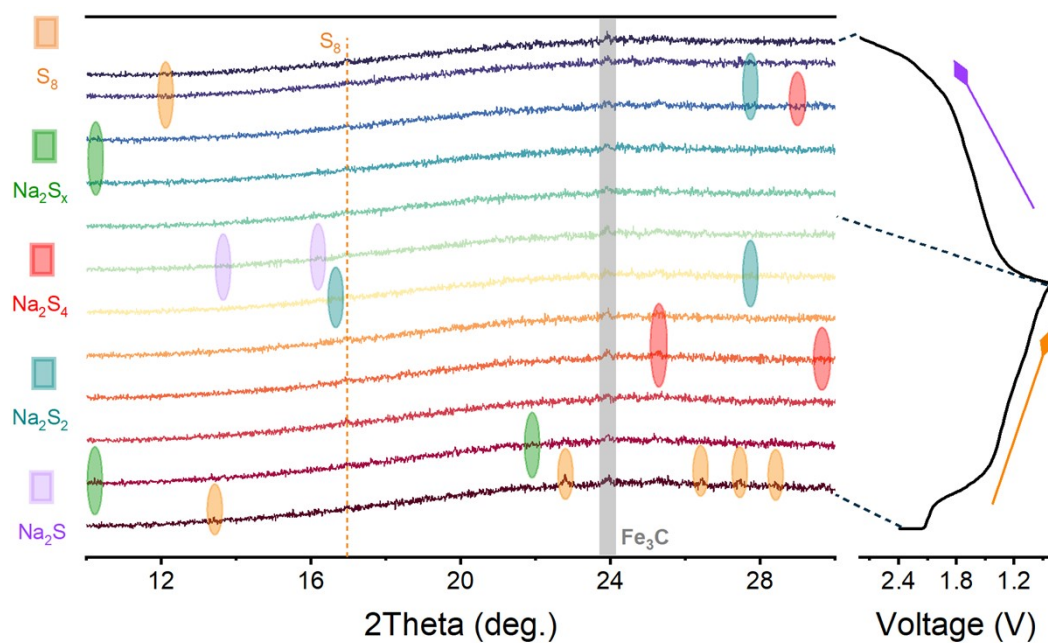


**Figure 16.** *In-situ* XRD patterns of the  $\text{Fe}_3\text{C}@\text{HPC-S}$  cathode along with discharge-charge profile at  $0.1 \text{ A g}^{-1}$ .

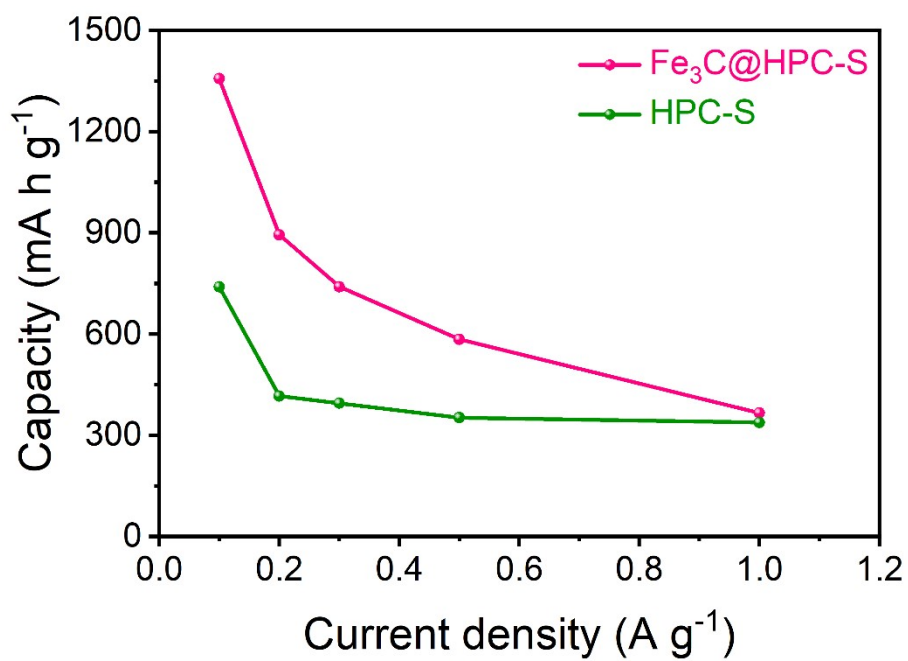


**Figure S17.** Rate capabilities of the Fe<sub>3</sub>C@HPC-S and HPC-S composite.

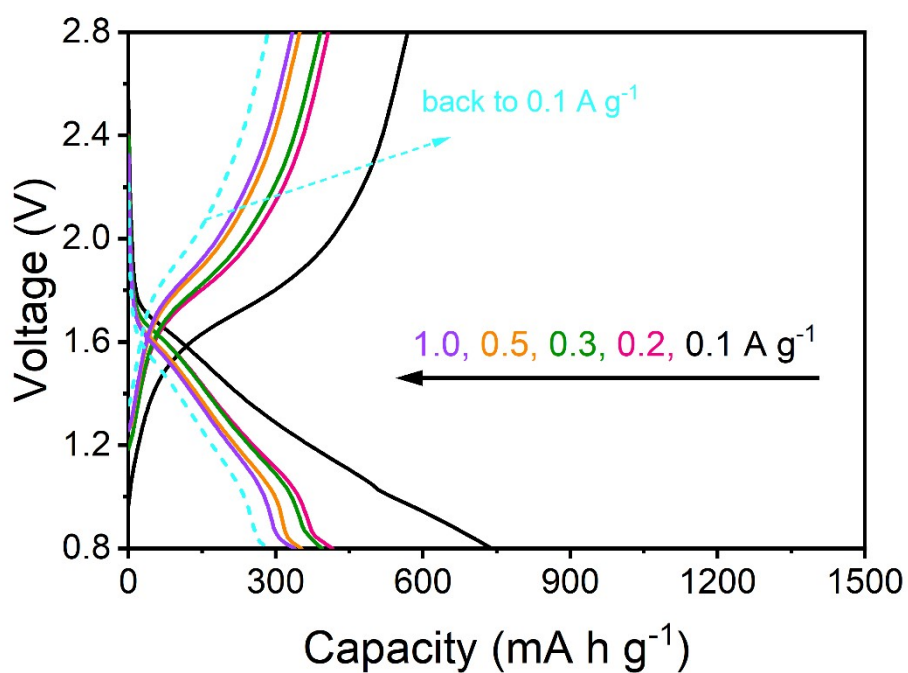


**Figure S18.** Discharge-charge profiles of the HPC-S composite.



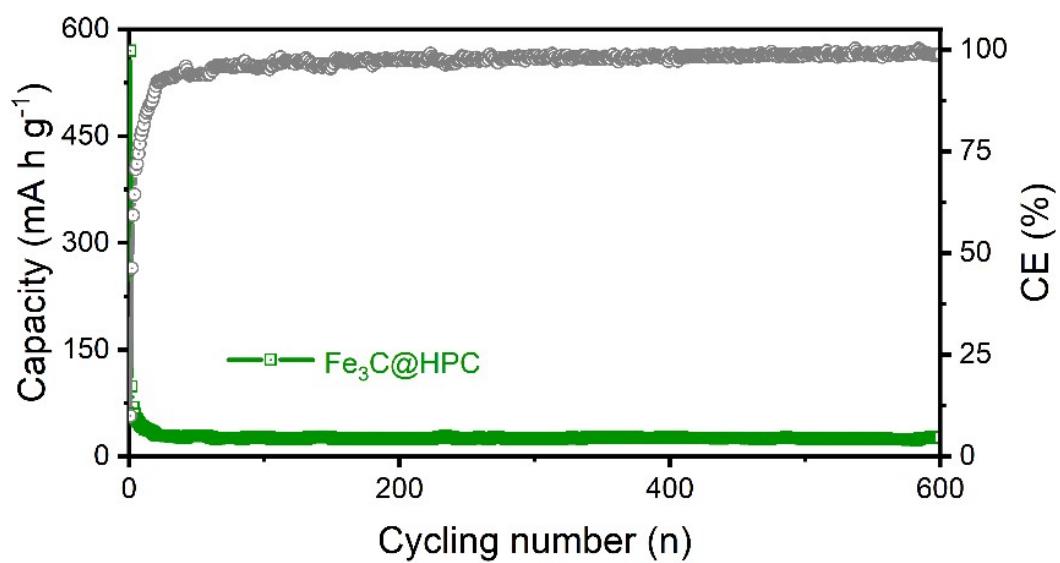


**Figure S20.** Cycling performance of the Fe<sub>3</sub>C@HPC at 1 A g<sup>-1</sup>.

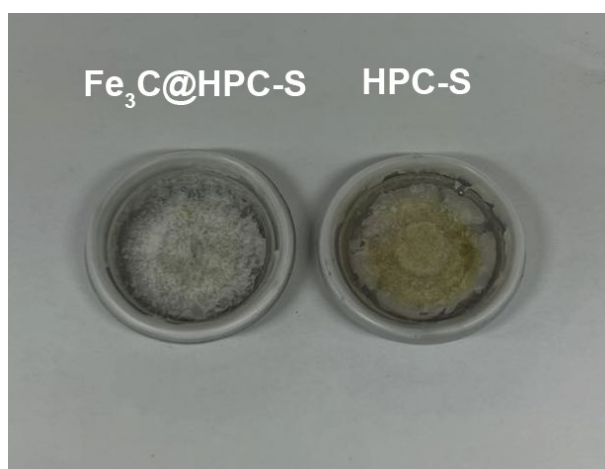


**Figure S21.** Comparison on Separators disassembled from RT Na-S batteries with different cathodes.

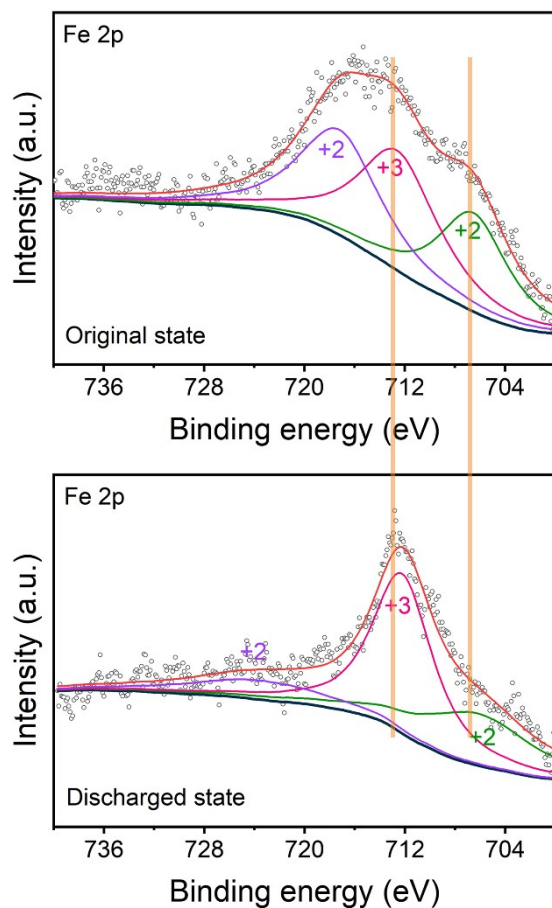


**Figure S22.** XPS spectra of the  $\text{Fe}_3\text{C}@HPC-S$  composite before and after discharging.

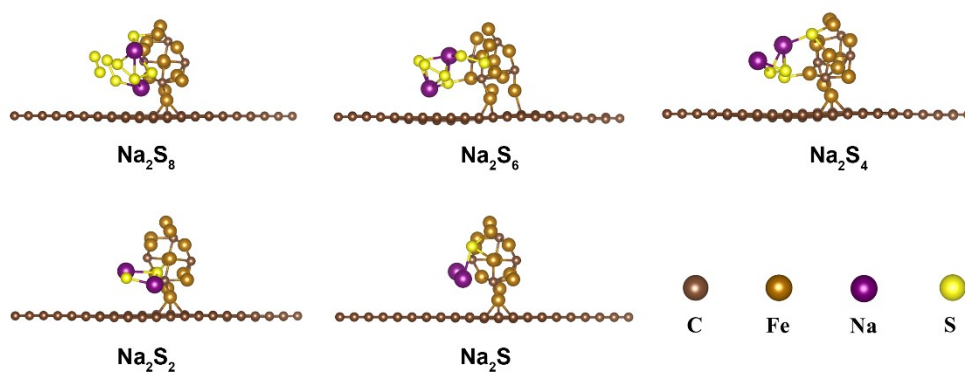


**Figure S23.** Typical adsorption configurations of  $\text{Na}_2\text{S}_n$  ( $n = 1, 2, 4, 6$  and  $8$ ) on the  $\text{Fe}_3\text{C}@HPC$  at a side view.

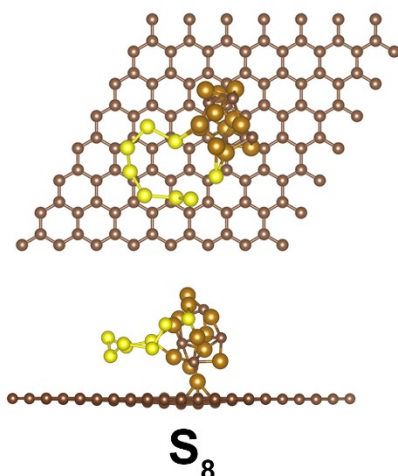


**Figure S24.** Typical adsorption configuration of  $S_8$  on the  $Fe_3C@HPC$  at the top and side view.

**Table S1.** The compilation of binding energies of sodium polysulfides ( $Na_2S_n$ ) on various anchoring materials.

System	Binding energies of $Na_2S_n$ (eV)					Reference
	$Na_2S$	$Na_2S_2$	$Na_2S_4$	$Na_2S_6$	$Na_2S_8$	
<b>Graphene</b>	<b>-0.82</b>	<b>-0.67</b>	<b>-0.51</b>	<b>-0.43</b>	<b>-0.33</b>	<b>Ref. [9]</b>
N-NPG	-2.77	-1.77	-1.37	-1.43	-1.66	Ref. [9]
$Fe@N_4$ -graphene	-1.09	-1.36	-1.07	-1.16	-1.35	Ref. [10]
$Ti_3C_2T_x$	---	-1.89	-2.88	-4.72	---	Ref. [11]
CoP-Co	-1.66	-1.74	-2.43	-2.66	---	Ref. [12]
$C_2N$	-3.09	-3.13	-2.51	-2.39	-2.33	Ref. [13]
$As_2S_3$	-3.26	-2.41	-1.94	-1.49	-1.52	Ref. [14]
<b><math>Fe_3C@graphene</math></b>	<b>-3.93</b>	<b>-3.54</b>	<b>-3.18</b>	<b>-2.96</b>	<b>-2.70</b>	<b>This work</b>

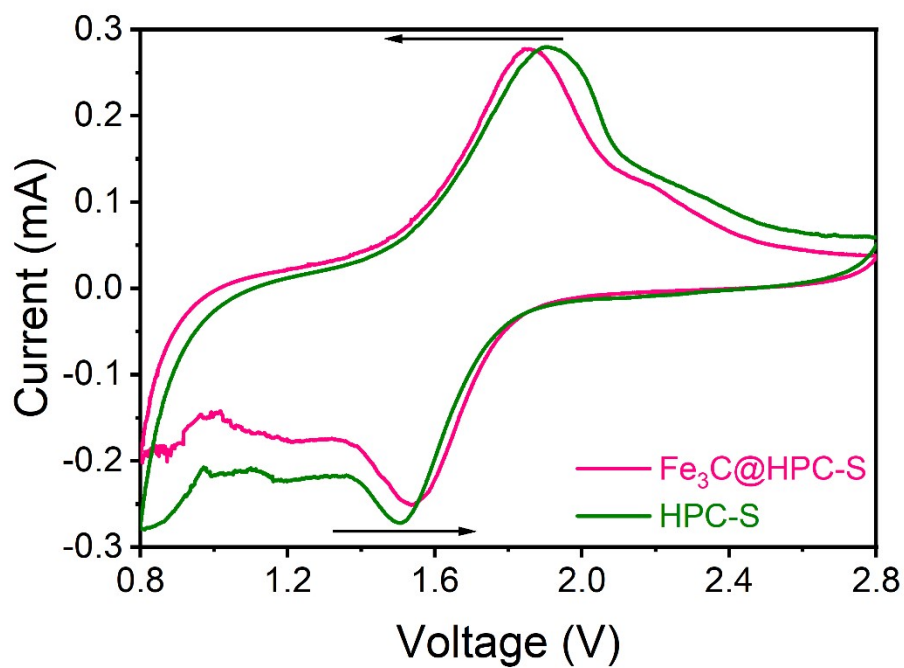


**Figure S25.** CV curves of the  $\text{Fe}_3\text{C@HPC-S}$  and HPC-S composite at the same scan rate.

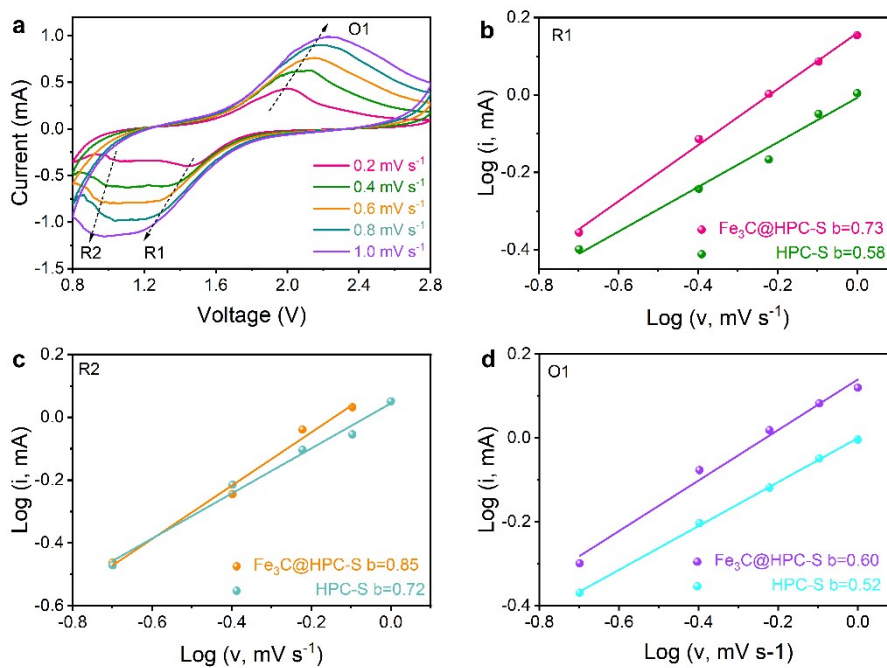


**Figure S26.** (a) CV curves of the HPC-S at different scan rates; (b-d) The linear relation of peak currents and scan rates.

As known, power-law equation ( $i = av^b$ ) is a good tool to determine the Na-ion diffusion behaviors, where  $a$  and  $b$  are the linear-fitted parameters ranging from 0.5 to 1.0, while  $i$  and  $v$  are redox peak current and sweep rate. The  $b$ -value can function as a direct indicator of electrochemical kinetics, since the electrochemical process is diffusion-controlled when  $b$  is closer to 0.5 but it is surface capacitance-dominant when  $b$  is closer to 1.0. According to two reduction peaks and an oxidation peak, the corresponding  $b$  values can be calculated, as shown in **Figure 23b-d**. Whether reduction or oxidation reactions, the  $b$  values from peaks of the Fe<sub>3</sub>C@HPC-S is higher than those of the HPC-S, indicating its faster Na ion diffusion and improved kinetics.

#### References:

1. G. Kresse, J. Furthmüller, Efficient Iterative Schemes for Ab Initio Total-Energy Calculations Using a Plane-Wave Basis Set. *Phys. Rev. B* **1996**, *54* (16), 11169–11186.
2. G. Kresse, J. Furthmüller, Efficiency of Ab-Initio Total Energy Calculations for Metals and Semiconductors Using a Plane-Wave Basis Set. *Comput. Mater. Sci.* **1996**, *6* (1), 15–50.
3. P. E. Blöchl, Projector Augmented-Wave Method. *Phys. Rev. B* **1994**, *50* (24), 17953–17979.
4. G. Kresse, D. Joubert, From Ultrasoft Pseudopotentials to the Projector Augmented-Wave Method. *Phys. Rev. B* **1999**, *59* (3), 1758–1775.
5. J. P. Perdew, K. Burke, M. Ernzerhof, Generalized Gradient Approximation Made Simple. *Phys. Rev. Lett.* **1996**, *77* (18), 3865–3868.
6. S. Grimme, Semiempirical GGA-Type Density Functional Constructed with a Long-Range Dispersion Correction. *J. Comput. Chem.* **2006**, *27* (15), 1787–1799.
7. H. J. Monkhorst, J. D. Pack, Special Points for Brillouin-Zone Integrations. *Phys. Rev. B*

1976, 13 (12), 5188–5192.

8. G. Henkelman, A. Arnaldsson, H. Jónsson, A Fast and Robust Algorithm for Bader Decomposition of Charge Density. *Comput. Mater. Sci.* **2006**, 36 (3), 354–360.
9. T. Hussain, T. Kaewmaraya, Z. Hu, X. S. Zhao, Efficient Control of the Shuttle Effect in Sodium–Sulfur Batteries with Functionalized Nanoporous Graphenes. doi.org/10.1021/acsanm.2c02405
10. T. Zhang, Z. Chen, J. Zhao, Y. Ding, Metal-N<sub>4</sub>/graphene as an efficient anchoring material for lithium-sulfur batteries: A computational study, *Diamond and Related Materials*, 90 (2018) 72-78.
11. W. Bao, C.E. Shuck, W. Zhang, X. Guo, Y. Gogotsi, G. Wang, Boosting Performance of Na–S Batteries Using Sulfur-Doped Ti<sub>3</sub>C<sub>2</sub>T<sub>x</sub> MXene Nanosheets with a Strong Affinity to Sodium Polysulfides, *ACS Nano*, 13 (2019) 11500-11509.
12. Z. Yan, Y. Liang, W. Hua, X.-G. Zhang, W. Lai, Z. Hu, W. Wang, J. Peng, S. Indris, Y. Wang, S.-L. Chou, H. Liu, S.-X. Dou, Multiregion Janus-Featured Cobalt Phosphide-Cobalt Composite for Highly Reversible Room-Temperature Sodium-Sulfur Batteries, *ACS Nano*, 14 (2020) 10284-10293.
13. M. Sajjad, T. Hussain, N. Singh, J.A. Larsson, Superior Anchoring of Sodium Polysulfides to the Polar C<sub>2</sub>N 2D Material: A Potential Electrode Enhancer in Sodium–Sulfur Batteries, *Langmuir*, 36 (2020) 13104-13111.
14. T. Kaewmaraya, T. Hussain, R. Umer, Z. Hu, X.S. Zhao, Efficient suppression of the shuttle effect in Na–S batteries with an As<sub>2</sub>S<sub>3</sub> anchoring monolayer, *Physical Chemistry Chemical Physics*, 22 (2020) 27300-27307.